Power Electronics and Drives
Volume 7(42), 2022 DOI: 10.2478/pead-2022-0018

Power Electronics and Drives

A Coordination Control between Battery and Supercapacitor Energy Storage Systems to Segregate Power for On-Grid Application

Research paper

Jeemut Bahan Sangiri[1,*], Supratik Bhowmick[2], Suman Maiti[2], Chandan Chakraborty[2]

[1]*School of Energy Science and Engineering, Indian Institute of Technology Kharagpur, Kharagpur, India*
[2]*Department of Electrical Engineering, Indian Institute of Technology Kharagpur, Kharagpur, India*

Received: September 22, 2022; Accepted: October 21, 2022

Abstract: The present work describes a control methodology for a hybrid energy storage system (HESS) to improve its transient performance under dynamic load conditions. The proposed coordination control enhanced life cycle performance by segregating the power between battery energy storage systems (BESS) and a supercapacitor (SC). The BESS and SC are connected parallel to each other, and two individual DC–DC bidirectional converters connect them to a common DC bus. The coordination control is established between the controllers of BESS and the SC of HESS, which helps to utilise the usable energy capacity of the HESS. The charging/discharging current of the BESS is controlled within the allowable safety range based on the slope and magnitude of the BESS current. The high-frequency power component is handled by the SC, which helps to reduce the extra exhaustion on the BESS during operation with a higher current. The proposed coordination control of HESS is validated through simulation and the results show the effectiveness of the proposed controller.

Keywords: *Hybrid energy storage system • battery control • power segregation • coordination control • energy management*

1. Introduction

Excessive usage of fossil fuels leads to environmental pollution, which may be reduced by using renewable energy sources (RES) and energy storage systems (ESS). In a real-life scenario, the power generation of RES and the power demanded by the load are intermittent in nature (Manandhar et al., 2018). The ESS plays an important role in power grid application, storing the energy when there is excess power and delivering it to the load when there is a requirement for power (Mukherjee and Strickland, 2016). Battery energy storage systems (BESS) are widely used and can store electrical energy in the form of chemical energy (Hredzak et al., 2014). Nowadays, lithium-ion (Li-ion) batteries are adopted in almost all kinds of applications because of their unique features, which are not readily available in other sources of power storage and dispensation; these include higher specific energy density, no memory effect, more cycling life, etc., and they help to make the battery pack possess a higher power handling capability (Abeywardana et al., 2017). A hybrid energy storage system (HESS) is an optimised solution involving the usage of a combination of two or more ESS that are of different time-constant elements (Ara´ujo et al., 2014). The supercapacitor (SC) is a special type of ESS that can store electrical energy through electric double-layer capacitance formed by charge separation on the interfaces of electrolytes and electrodes (Huang et al., 2017; Kollimalla et al., 2017; Henz and Gasparin, 2021). Incorporation of SC with the BESS can improve the capability of the HESS, imbibing it with higher energy and power density, which is suitable for applications involving higher charge/discharge rates; therefore, a hybrid energy storage consisting of BESS and SC is considered for this study. A proper control methodology should be followed to manage average and transient power among the BESS and

* *Email: jeemut@iitkgp.ac.in*

SC elements during the step-changed load (Hredzak et al., 2014; Mukherjee and Strickland, 2016; Abeywardana et al., 2017).

Generally, BESS is preferred to deliver a nominal amount of power to the load, but sometimes, it cannot meet the requirement of high transient peak power demand due to its slow dynamic response (Jossen, 2006). The requirement of grid power is not in a constant long timescale because of peak load demand at the consumer side during some intervals of the day (Ara´ujo et al., 2014; Łukasz and Zieliński, 2021). SC ESS devices can take care of higher transients of the power requirement for a shorter time duration. So, the combination of BESS and SC devices can deliver power to the transient and steady-state parts of the load profile of the grid with the help of the proposed coordination algorithm between the BESS and SC controllers (Lahyani et al., 2013; Ma et al., 2015). The state of health of the BESS is an important factor to be observed during the operation, as SOH denotes the performance of BESS.

HESSs of different time scales constitute a major concern nowadays as compared to the single-type ESS (Manandhar et al., 2018). HESS is widely accepted in electric vehicles as well as for grid-tied ESS (Hredzak et al., 2014; Abeywardana et al., 2017). A combination of two or more ESS can help to improve the system performance for power grid applications. An appropriate control strategy needs to be incorporated to distribute the power requirements among the ESS present in the HESS. To effectively control the average and dynamic power sharing between SC and BESS, several strategies are followed in the literature. A model-based two-state limitation is followed to implement the control algorithm between BESS and SC (Mukherjee and Strickland, 2016). A control strategy was proposed and designed for a single-phase DC/AC on-grid converter to improve the efficiency of the photovoltaic array (Amin et al., 2014). A generic battery model is used for the dynamic simulations of the electric vehicles (Tremblay et al., 2007). Neural networks and fuzzy logic (Kollimalla et al., 2017) have been used in HESS to control power segregation between the BESS and SC elements. However, a high computing facility is needed for this type of controller. The combination of the fuel cell, BESS, and SC is used to form HESS (Dusmez and Khaligh, 2014). These types of HESS combination are useful for standalone microgrid as well as application in electric vehicles.

In this work, SCs are added with the BESS to design a HESS of high energy and power density. A coordination control strategy is proposed between BESS and SC to segregate the higher and lower frequency components of the grid power. The incorporation of the gain factor in the control loop of SC reference current generation accelerates the process of compensating for the power mismatch at the DC bus because of the slow dynamics of BESS during transient operation. This gain factor helps in improving the transient response of HESS subjected to any dynamic load change condition and therefore makes the HESS have a faster response subjected to any load change at the utility grid. A stability analysis based on the root-locus plot of the system is carried out to find the range of the gain factor for system stability and then select a suitable gain factor value.

The remainder of this paper is organised as follows: Section 2 describes the detailed system configuration of the proposed HESS used for this study. Section 3 describes the proposed control strategies used for segregating average and transient power between the BESS and SC. The stability analysis based on the root-locus plot of the proposed coordination control system is also detailed in this section. The obtained results, along with the discussion, are presented in Section 4. Finally, the conclusions of this work are presented in Section 5.

2. System Configuration

The system configuration of the proposed coordination control-based HESS fed grid-tied inverter is shown in Figure 1.

A HESS is considered, which consists of BESS and SC ESS. BESS and SC are connected in parallel to each other to form a common DC bus with the help of two DC–DC bidirectional boost converters, individually connected in series with BESS and SC. The DC bus is connected with the 3-Φ grid through a three-phase two-level inverter and a passive LCL filter.

The grid-tied inverter is controlled in dq reference frame in order to inject a specified amount of active and reactive power into the grid, and this commands the amount of average DC link current that needs to be supplied from the HESS. If the charge/discharge current exceeds the limiting value of the battery current, then SC will be turned on, thus taking care of the higher requirement of power demand.

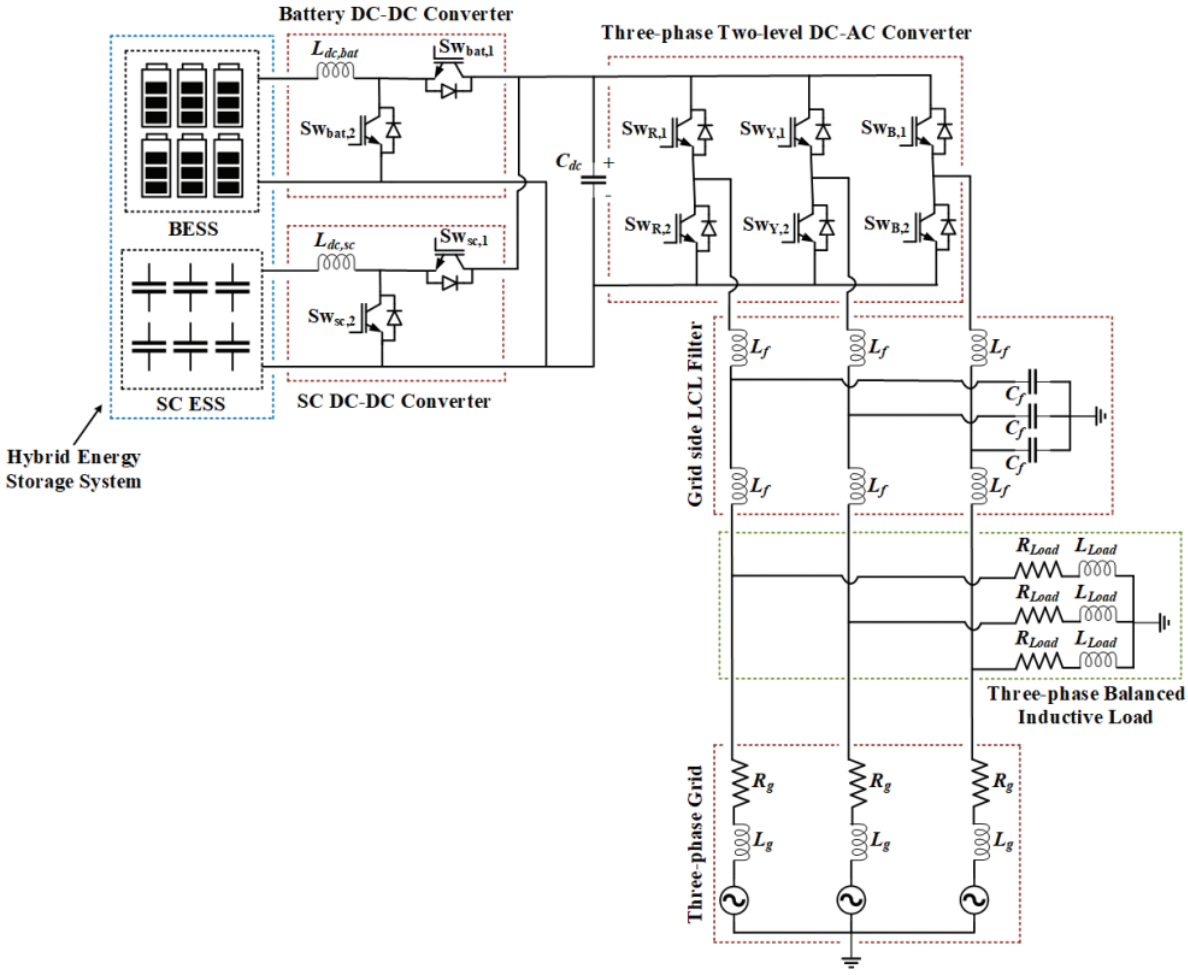

Fig. 1. Schematic diagram of the system with batteries and SCs as energy storage devices. SC, supercapacitor.

3. Proposed Control Mechanism

The overall control mechanism of the power-electronic converters in the system, as shown in Figure 1, consists of coordination control between the BESS and SC ESS in the HESS and the inverter control in the decoupled double synchronous reference frame (DDSRF) using instantaneous power theory (Akagi et al., 1984; Aredes and Watanabe, 1995). This paper considers an improved coordination control of BESS and SC ESS based on incorporating a gain factor in the control loop of SC reference current generation without losing the system stability.

The block diagram of conventional coordination control of HESS is shown in Figure 2. The reference battery current is determined from the commanded DC link current by filtering out the AC components and the PI controller for the battery, while the DC–DC converter ensures that the actual current of the battery (i_{bat}) reaches its reference value in steady state.

To generate the reference current for the SC ESS, the uncompensated power due to the error current in the battery controller is utilised during transient conditions since the total DC link power needs to satisfy the grid power, neglecting losses in the grid-tied inverter and non-ideal components of the grid side filtering elements. The uncompensated power during transient conditions till the time the battery current reaches its steady-state value is obtained as follows:

$$P_{uncomp}(t) = i_{bat,err}(t) \times v_{bat}(t) = \left(i_{bat,ref} - i_{bat}(t)\right) \times v_{bat}(t) \quad (1)$$

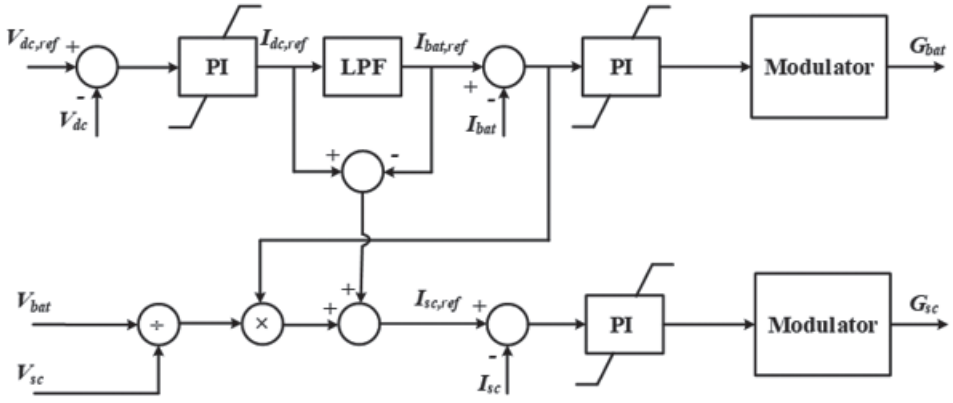

Fig. 2. Conventional controller block diagram of the system with batteries and SCs as energy storage devices. SC, supercapacitor.

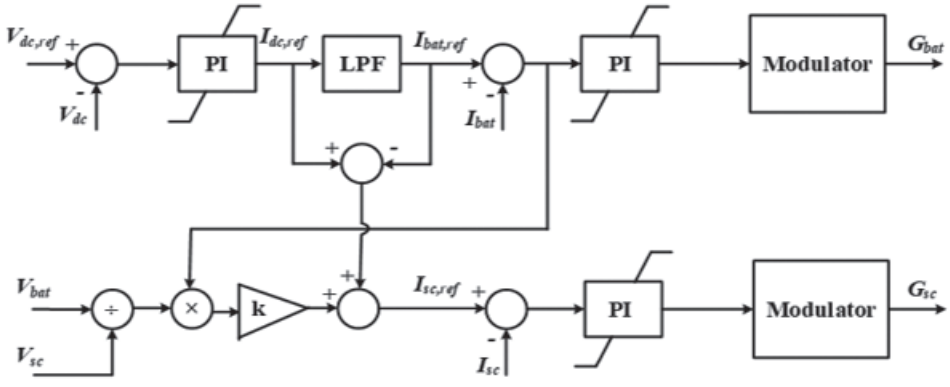

Fig. 3. Proposed controller block diagram of the system with batteries and SCs as energy storage devices. SC, supercapacitor.

The reference current for the SC controller can therefore be obtained from Eq. (1) as follows:

$$i_{sc,ref}(t) = \left(i_{bat,ref} - i_{bat}(t)\right) \times \frac{v_{bat}(t)}{v_{sc}(t)} \tag{2}$$

It is important to mention that the compensation of $P_{uncomp}(t)$ is essential because of the slow dynamics of the battery system and therefore the power imbalance may sustain for a significant amount of time.

Incorporation of gain factor '*k*'

In order to accelerate the process of compensating the uncompensated power ($P_{uncomp}(t)$) during transient operation, a gain factor *k* is introduced along with the ratio $\left(\frac{v_{bat}(t)}{v_{sc}(t)}\right)$ for generating the reference current of SC ESS. The reference current expression for SC ESS therefore becomes:

$$i_{sc,ref}(t) = \left(i_{bat,ref} - i_{bat}(t)\right) \times k \times \frac{v_{bat}(t)}{v_{sc}(t)} \tag{3}$$

The proposed block diagram after incorporating the gain factor *k* is shown in Figure 3. The introduction of gain factor *k* in the coordination control accounts for an unstable region, and therefore it is important to judiciously select

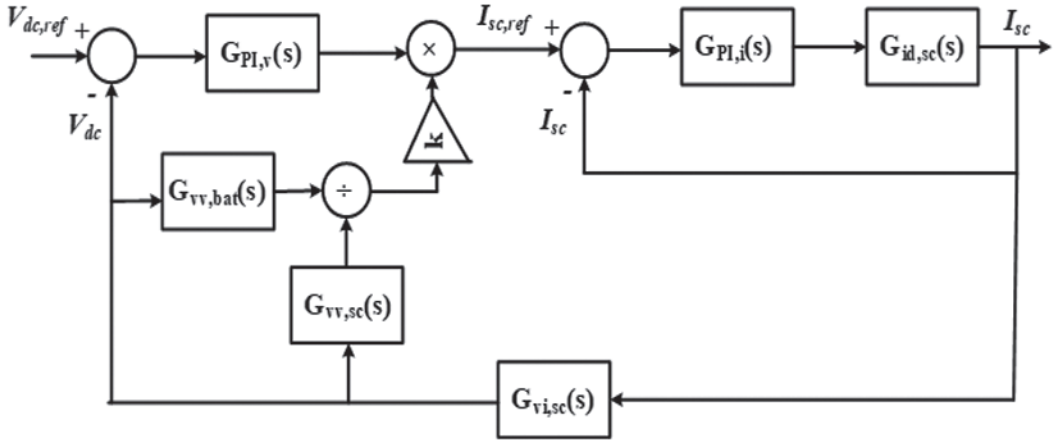

Fig. 4. Closed-loop block diagram for controlling SC ESS. ESS, energy storage systems; SC, supercapacitor.

the value of *k* for improved performance of the system without losing the system stability. This subsection, therefore, analyses the effect of gain factor *k* in the coordination control between BESS and SC ESS.

Following Figure 3, the closed-loop block diagram of the SC controller is demonstrated in Figure 4. The transfer functions of battery and SC bidirectional DC–DC converters can be obtained from a small-signal analysis of these converters, and are expressed as follows:

$$G_{vv,bat}(s)=\frac{\hat{v}_{bat}(s)}{\hat{v}_{dc}(s)}=\frac{\left\{\left(L_{bat}C_{bat}\right)s^2+\left(L_{bat}/R_L\right)s+\left(1-D_{bat}\right)^2\right\}}{\left(1-D_{bat}\right)} \tag{4}$$

$$G_{vv,sc}(s)=\frac{\hat{v}_{sc}(s)}{\hat{v}_{dc}(s)}=\frac{\left\{\left(L_{sc}C_{sc}\right)s^2+\left(L_{sc}/R_L\right)s+\left(1-D_{sc}\right)^2\right\}}{\left(1-D_{sc}\right)} \tag{5}$$

$$G_{vi,sc}(s)=\frac{\hat{v}_{dc}(s)}{\hat{i}_{Lsc}(s)}=\frac{\left\{-\left(V_{dc}L_{sc}/R_L\right)s+V_{dc}\left(1-D_{sc}\right)\right\}}{\left\{\left(C_{sc}V_{dc}\right)s+\left(V_{dc}/R_L\right)\left(2-D_{sc}\right)\right\}} \tag{6}$$

$$G_{id,sc}(s)=\frac{\hat{i}_{Lsc}(s)}{\hat{d}_{sc}(s)}=\frac{\left\{\left(C_{sc}V_{dc}\right)s+\left(V_{dc}/R_L\right)\left(2-D_{sc}\right)\right\}}{\left\{\left(L_{sc}C_{sc}\right)s^2+\left(L_{sc}/R_L\right)s+\left(1-D_{sc}\right)^2\right\}} \tag{7}$$

where L_{bat} and L_{sc} are input inductances of battery and SC bidirectional DC–DC converters, respectively; C_{bat} and C_{sc} are output capacitances of battery and SC bidirectional DC–DC converters, respectively; D_{bat} and D_{sc} are average duty ratios generated for battery and SC bidirectional DC–DC converters, respectively, at steady state; V_{dc} is average DC link voltage at steady state; and R_L is a virtual resistive load at DC bus, i.e. $R_L=\frac{V_{dc}^2}{P_{dc}}$. The detailed mathematical derivation of the transfer function equations are available in Appendix.

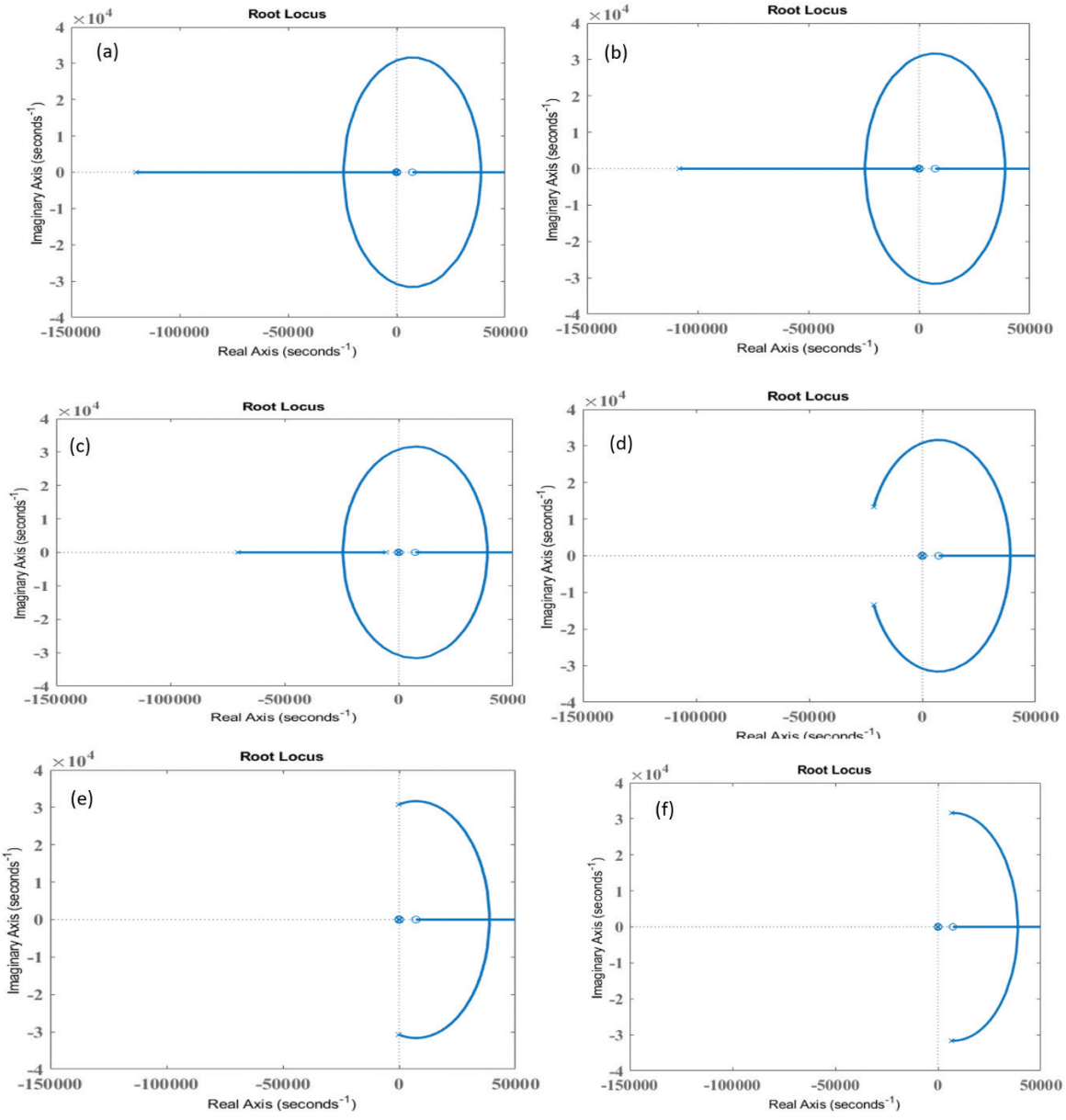

Fig. 5. Root-locus plots of SC controller loop transfer function for (a) $k = 1$, (b) $k = 2$, (c) $k = 5$, (d) $k = 8$, (e) $k = 11.86$ (boundary condition), and (f) $k = 12$. SC, supercapacitor.

The loop transfer function of the SC control loop as shown in Figure 4 can therefore be obtained as:

$$G_{loop,sc}(s) = k \times \frac{G_{vv,bat}(s)}{G_{vv,sc}(s)} \times G_{cl,isc}(s) \times G_{vi,sc}(s) \tag{8}$$

$$\text{where, } G_{cl,isc}(s) = \frac{G_{PI,i}(s) \times G_{id,sc}(s)}{\left\{1 + G_{PI,i}(s) \times G_{id,sc}(s)\right\}} \tag{9}$$

The root-locus plot of the loop transfer function $G_{loop,sc}(s)$ are obtained for different values of gain factor k in Figure 5. It can be observed from Figure 5e that the system becomes marginally stable for $k = 11.86$, which confirms

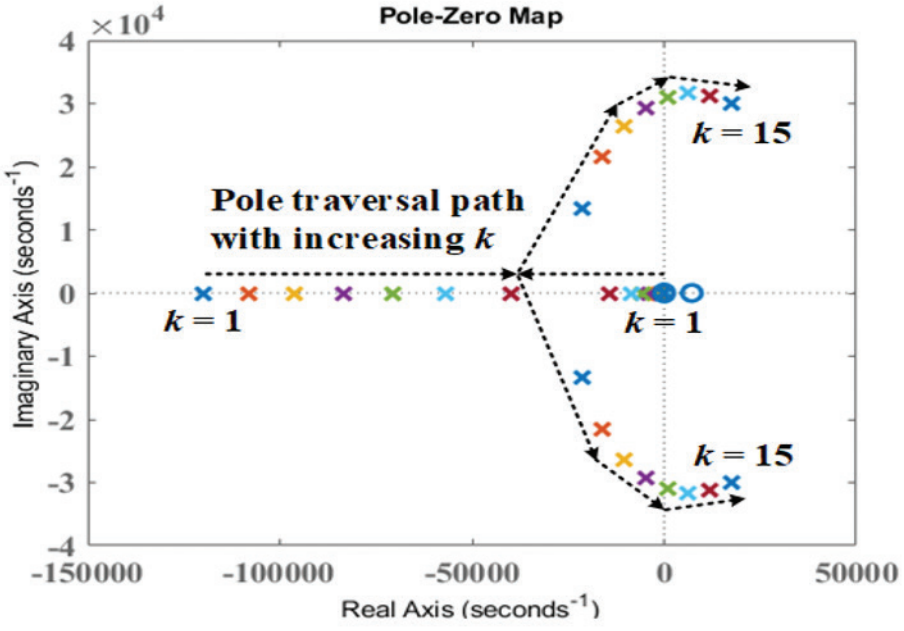

Fig. 6. Pole zero map of SC controller loop transfer function for variation of k from 1 to 15. SC, supercapacitor.

the boundary condition of stability. Also, from Figure 5d, we ascertain that for $k = 8$, the poles of $G_{loop,sc}(s)$ no longer remain on the negative real axis, which confirms the oscillatory nature in the dynamic response of the system. The dynamic performance of HESS that is controlled by the proposed coordination method for these gain factor values are explained in the next section. Figure 6 shows how the poles and zeros traverse when the gain factor k is varied from 1 to 15.

4. Results and Discussions

In this work, the HESS is controlled by using coordination control between the controllers of inverter, batteries, and SCs to achieve the load demand from the utility grid. The converter-inverter system is simulated first with the conventional closed-loop coordination control of BESS and SC ESS. The complete system is simulated using MATLAB/Simulink software and the parameters of the system are given in Table 1. The block diagram for the complete system that is used for simulation is given in Figure 7. The results are shown in Section 4.1 for step load change. The SC renders major support to balance the load-demand characteristics because of its higher charge/discharge cycles. The results are shown for SC current, voltage, and SoC change for step change in reference grid active power and a detailed analysis is available in Section 4.2.

4.1. Conventional coordination control of BESS and SC ESS for a step change in reference grid power

A load of a power grid is not fixed, and based on the requirement it may vary with time. Mainly, there are two cases possible for a step change in the load; connection of load at point of common coupling (PCC) of utility grid and disconnection of load from utility grid. These two case studies are considered in this section and the corresponding results are discussed in the subsections of this section.

4.1.1. Case study-1: Connection of balanced load at PCC of grid

In this case study, a three-phase balanced inductive load of R_{Load} = 12.1 Ω and L_{Load} = 5 mH in each phase has been connected at the PCC of the utility grid to show the dynamic performance of the discussed

Specifications of BESS:
Nominal voltage = 360 V Rated capacity = 66.67 A·h Initial state-of-charge = 100% Fully charge voltage = 388 V Internal resistance = 0.013 Ω
Specifications of SC ESS:
Rated capacitance = 500 F Equivalent DC series resistance = 2.1 mΩ Rated voltage = 360 V Number of series capacitors = 6 Number of parallel capacitors = 1
Specifications of battery and SC based DC–DC converter:
Input inductance = 50 mH Switching frequency = 10 kHz
Specifications of grid side three-phase two-level inverter:
DC link capacitance = 4.7 mF Switching frequency= 10 kHz
Specifications of three-phase utility:
Filter inductance = 20 mH Filter capacitance = 1 μF Line-to-line grid voltage = 110 V (rms) Per phase grid impedance = (0.6 + j0.974) Ω

BESS, battery energy storage systems; ESS, energy storage systems; SC, supercapacitor.

Table 1. Specification of system parameters.

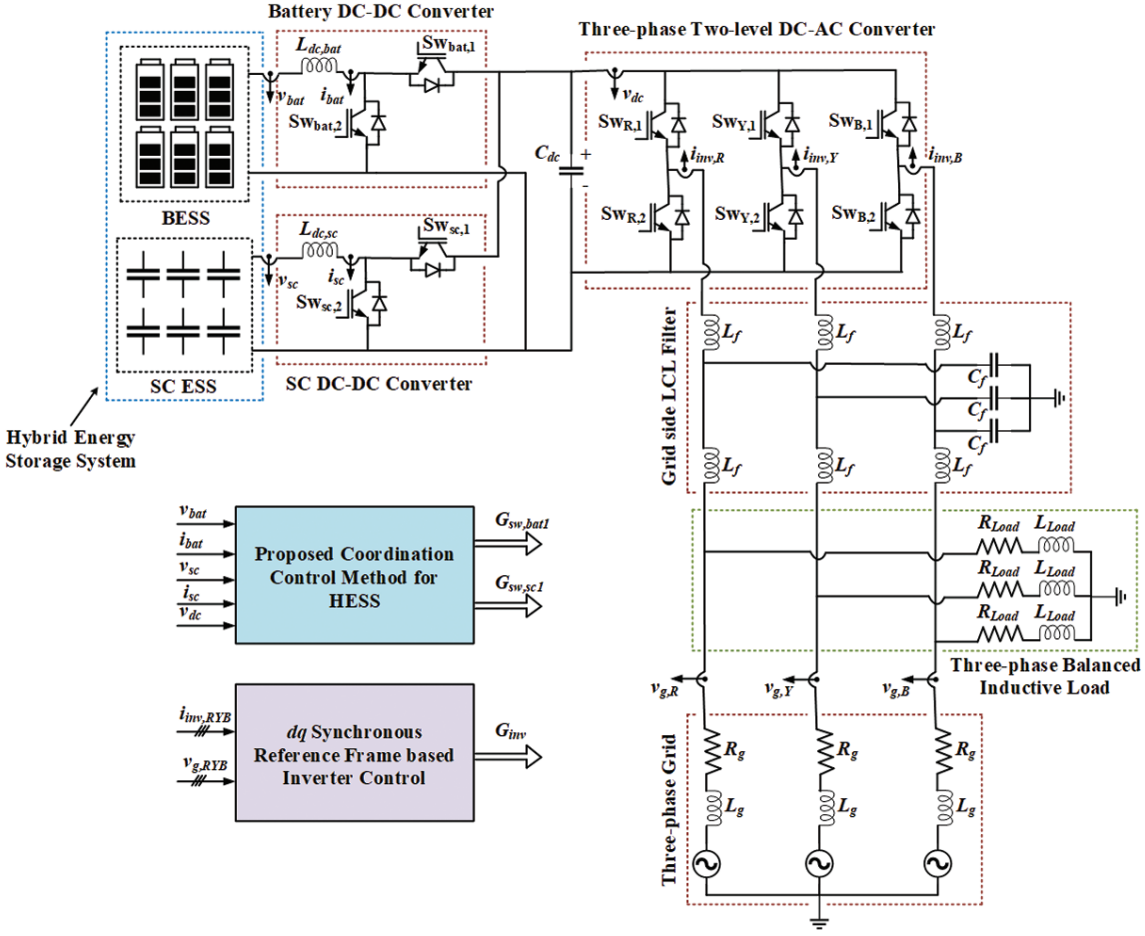

Fig. 7. Schematic diagram of the battery and super capacitor based HESS grid-connected system. HESS, hybrid energy storage system.

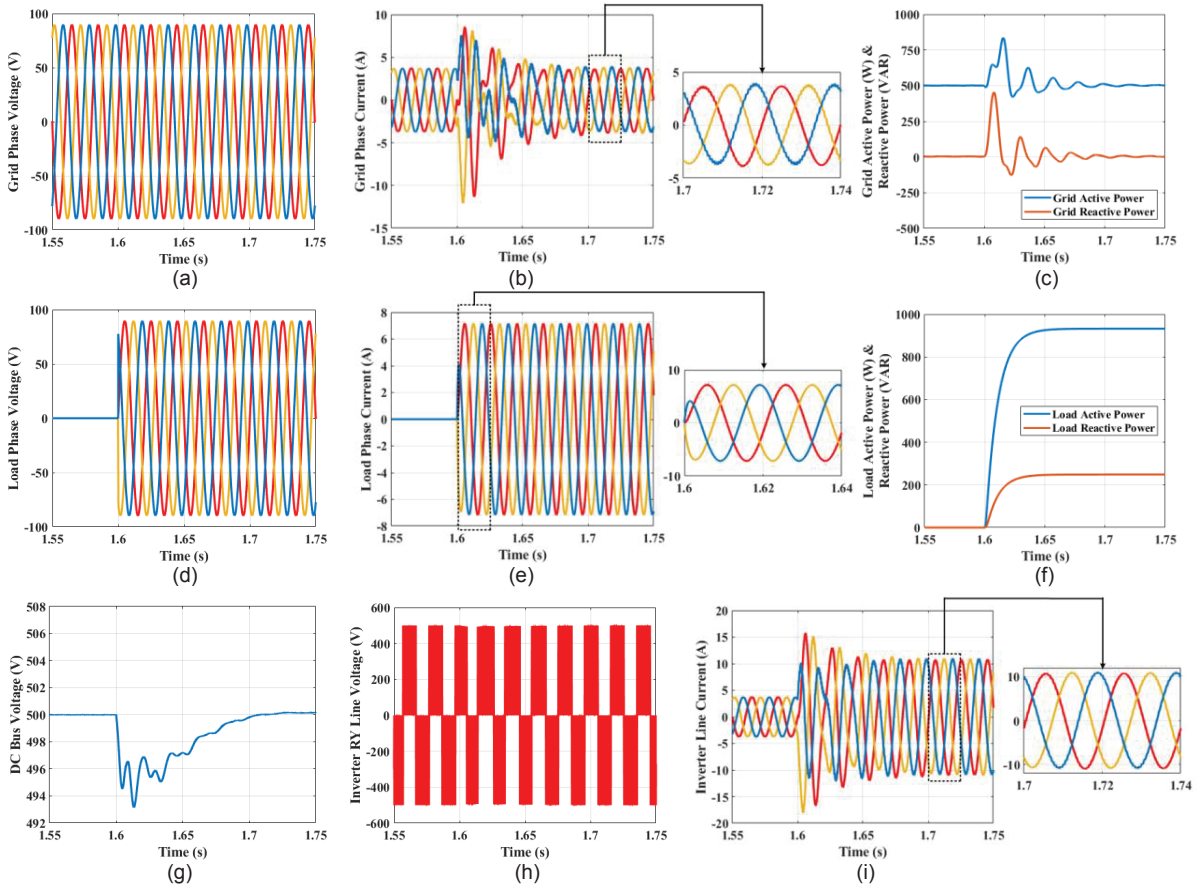

Fig. 8. Simulation results showing variation of (a) grid phase voltage, (b) grid phase current, (c) grid active and reactive power, (d) load phase voltage, (e) load phase current, (f) load active and reactive power, (g) DC bus voltage, (h) inverter RY line voltage, and (i) inverter line current for connection of a three-phase balanced load at PCC of the grid.PCC, point of common coupling.

power-semiconductor-based converter-inverter system. The grid power is maintained at constant 0.5 kW at unity power factor (upf) throughout the operation and at 1.6 s, the three-phase load is connected at the PCC of grid. The grid phase voltages and currents are shown in Figures 8a,b, where it is noticed that there is no change in the phase voltages and currents of the grid at steady state. The grid active and reactive power remain at 0.5 kW and 0 kVAR, respectively, even after connecting the load at PCC (Figure 8c). The load phase currents are observed to be balanced and lagging in nature, which starts from 1.6 s, ensures the connection of the required load into the system (Figure 8e). The DC bus voltage and the output line voltage for the grid side three-phase two-level inverter are shown in Figures 8g,h. The three-phase inverter line current waveform shows that before connection of the three-phase load, the inverter supplies only the grid current and once the load is connected into the system, the inverter injects summation of the load current and the grid current, which ensures proper working of the inverter controller (Figure 8i).

The power of the BESS and SC are varying when the active power requirement is changed from 0.5 kW to 1.5 kW (because of connection of the load). The coordination control has been implemented between the controllers of the inverter, BESS, and SC, which helps to manage the power demand by segregating the required power among the BESS and SC devices. The simulation results of BESS and SC currents are shown in Figure 9a, the powers of BESS and SC are shown in Figure 9b, and battery voltage for connection of the three-phase load at 1.6 s is shown in Figure 9c. It is observed that the SC can contribute to handling a higher transient part of the load cycle, and then its current becomes zero when the battery current reaches its desired magnitude at steady state.

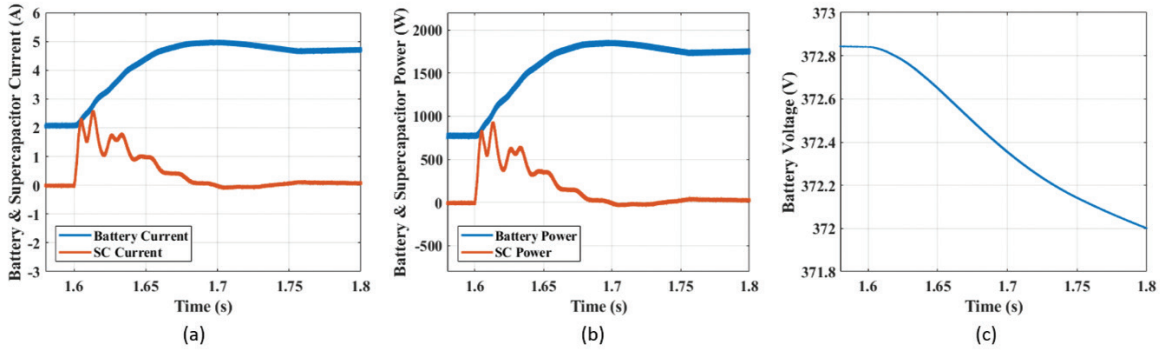

Fig. 9. Simulation results showing variation of (a) battery and SC current, (b) battery and SC power, and (c) battery voltage for connection of a three-phase balanced load at PCC of the grid. PCC, point of common coupling. SC, supercapacitor.

4.1.2. Case study-2: For disconnection of balanced load at PCC of grid

Another case study has been done when the three-phase balanced inductive load has been disconnected from the PCC of utility grid. In this case study, the three-phase load is disconnected at 1.8 s and the results are analysed. The 3-Θ voltages and currents of the grid are shown in Figure 10a, where it is demonstrated that there is no change in the phase voltages and currents at steady state (Figures 10a,b). The active and reactive power of the grid are shown in Figure 10c, and it is noticed that both the grid active and reactive powers maintain their respective values once the system reaches steady state. The phase voltages of the load is shown in Figure 10(d). The load phase currents become zero at 1.8 s, confirming that the load is disconnected from the system (Figure 10e). The DC link voltage of the inverter is shown in Figure 10g, where it is noticed that following an overshoot of 1.16%, the DC link stabilises at 1.92 s, which is within 0.12 s of the load change applied. The inverter RY line voltage is shown in Figure 10h and the line current of the inverter is shown in Figure 10f, and from these we ascertain that the inverter supplies only the grid current once the load is disconnected from the system. The line current of the inverter is shown in Figure 10(i), for disconnection of a three-phase balanced load at PCC of the grid.

The controllers of BESS and SC can establish coordination control among themselves, which helps to segregate the power between BESS and SC based on the power requirement. The battery and SC currents are shown in Figure 11a, where it is observed that the battery current comes down to 2 A from 4.8 A, and during this transition, SC consumes power and can be charged accordingly, as shown in Figure 11b. The battery voltage is shown in Figure 11c, where initially a decrease in battery voltage is observed and after 1.8 s an increase in battery voltage is observed, as the charging operation happens at this time. The slow dynamics of the BESS make the voltage response system slower, as shown in Figure 11c.

4.2. Effect of gain factor k on SC current and DC bus voltage

A gain factor, k, is added to the conventional controller to make it more accurate and precise. Since the gain factor can accelerate the power compensation by SC ESS due to the sluggish response of BESS, it is important to obtain the range of k to improve the dynamic performance of HESS without violating the system stability. The gain factor k is selected based on the system stability response. Stability analysis based on a root-locus plot has been performed, and the system response is observed for different values of k, as shown in Figure 12.

The values of k are chosen as $k = 1$, $k = 2$, $k = 5$, $k = 8$, and $k = 12$, and grid active power, battery current, SC current, and DC bus voltage for each of the cases are plotted individually. As seen in Figure 12, it can be concluded that the system becomes unstable for the gain factor $k = 12$, since it is established in Subsection 3.1 that the critical gain factor (k_{cri}) for marginal stability of the system is 11.86. Also, from Figure 12c,d and as described in Subsection 3.1., the oscillatory nature of the system is reflected in SC current and DC bus voltage, corresponding to gain factor values of k = 5 and 8.

The SC ESS response for the different k values as considered for the root-locus plots are tabulated in Table 2. It is important to mention that the transient response of the DC link voltage gets affected by the SC ESS response and therefore a similar investigation is carried out for DC link voltage. From our investigation into the considered

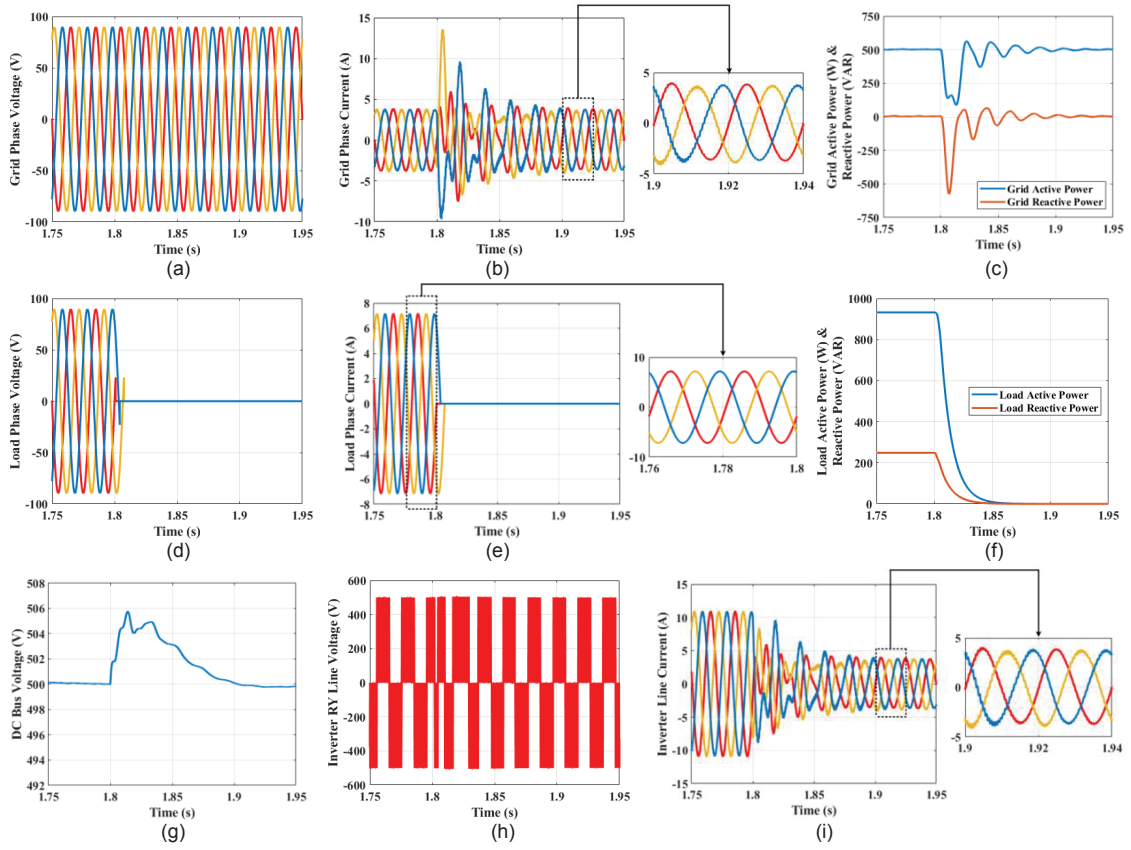

Fig. 10. Simulation results showing variation of (a) grid phase voltage, (b) grid phase current, (c) grid active and reactive power, (d) load phase voltage, (e) load phase current, (f) load active and reactive power, (g) DC bus voltage, (h) inverter RY line voltage, and (i) inverter line current for disconnection of a three-phase balanced load at PCC of the grid. PCC, point of common coupling.

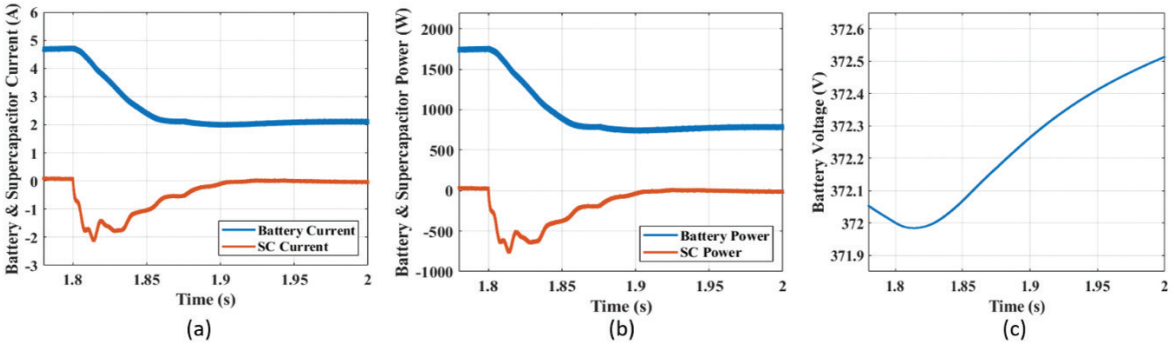

Fig. 11. Simulation results showing the variation of (a) battery and SC current, (b) battery and SC power, and (c) battery voltage for disconnection of a three-phase balanced load at PCC of the grid. PCC, point of common coupling; SC, supercapacitor.

parameters of SC current and DC bus voltage based on the values tabulated in Table 2, we infer that an optimal selection of gain factor $k = 2$ can be chosen for the better transient performance of the proposed coordination control.

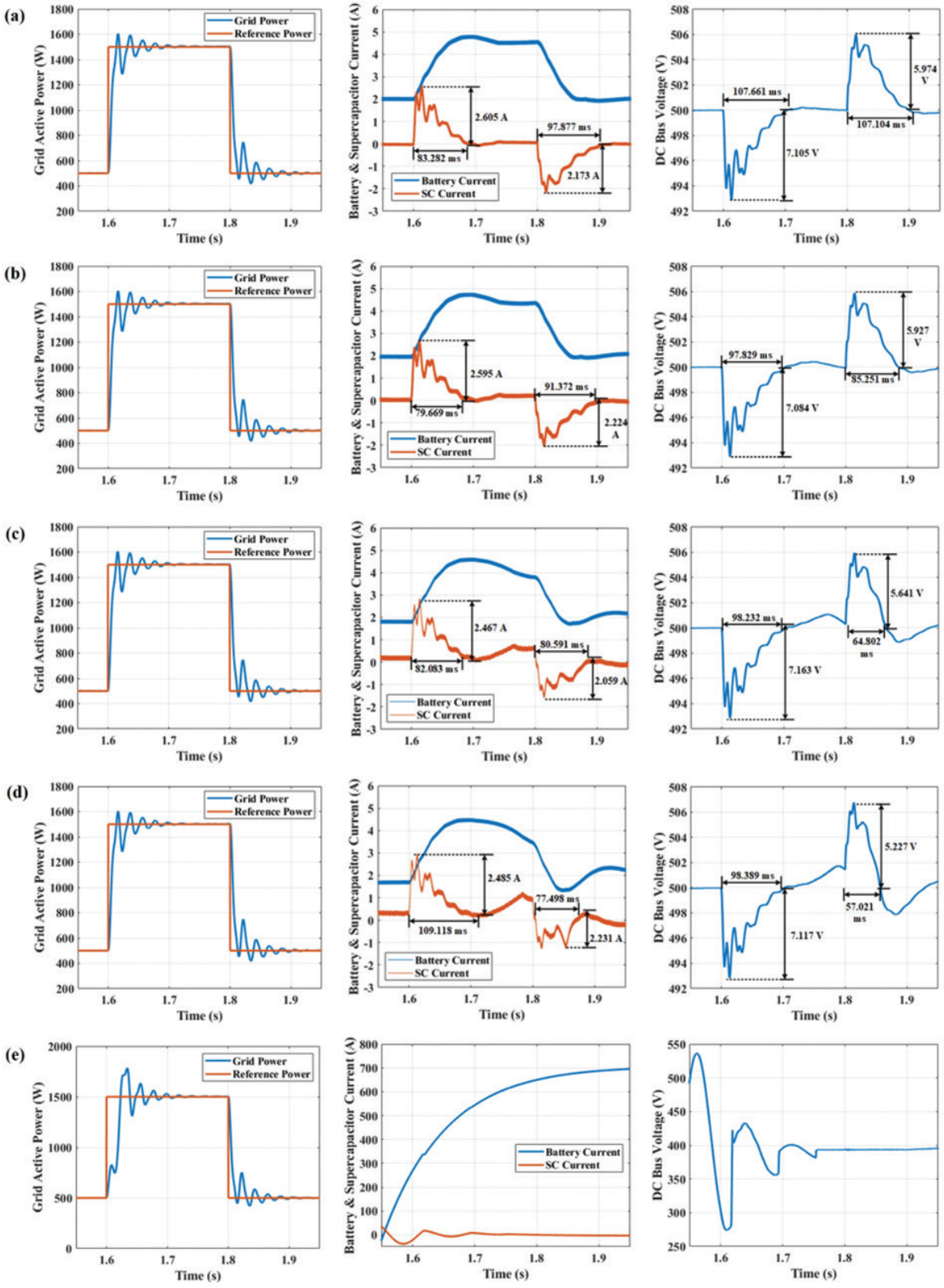

Fig. 12. Simulation results showing grid active power, battery and SC current, and DC bus voltage for (a) $k = 1$, (b) $k = 2$, (c) $k = 5$, (d) $k = 8$, and (e) $k = 12$. SC, supercapacitor.

Gain factor, k	SC peak current during on transition (A)	SC current on-settling time (ms)	SC peak current during off transition (A)	SC current off-settling time (ms)	DC bus voltage on transition (V)	DC bus voltage settling time for on transition (ms)	DC bus voltage off transition (V)	DC bus voltage settling time for off transition (ms)	System Stability
$k = 1$	2.605	83.287	2.173	97.877	7.105	107.661	5.974	107.104	Yes
$k = 2$	2.595	79.669	2.224	91.372	7.084	97.829	5.927	85.251	Yes
$k = 5$	2.467	82.083	2.059	80.591	7.163	98.232	5.641	64.802	Yes
$k = 8$	2.485	109.118	2.231	77.498	7.117	98.389	5.227	57.021	Yes
$k = 12$	-	-	-	-	-	-	-	-	No

SC, supercapacitor.

Table 2. SC current and DC link voltage response parameters for different values of gain factor k.

5. Conclusions

In this study, a coordination control methodology has been proposed for a HESS, consisting of BESS and SC ESS. The operating current limit of the BESS is maintained within the allowable safety limit, which reduces the chance of battery deterioration and helps to improve the cycle-life of the battery. The remaining amount of current and compensation of unmatched power during transient operation is taken care of by the SC ESS. The transient performance of HESS is improved by incorporating a gain factor to accelerate the process of unmatched power compensation by SC ESS. The dynamic performance of HESS, at the time it is subjected to sudden load change at the utility grid, is studied when HESS is controlled by the proposed coordination method for different gain factor values that are simulated; and an investigation into the various system parameters results in an optimal selection of gain factor for the proposed coordination control. A stability analysis based on the root-locus plot of the system is carried out to find the range of the gain factor for system stability. The simulation results are observed to be accurate with the developed mathematical analysis and the root-locus plot study, and therefore the proposed coordination control-based power segregation method ensures that the HESS is capable of improved performance when it undergoes any load transient operation.

References

Abeywardana, D. B. W., Hredzak, B. and Agelidis, V. G. (2017). A Fixed Frequency Sliding Mode Controller for a Boost-Inverter-Based Battery Supercapacitor Hybrid Energy Storage System. *IEEE Transactions on Power Electronics*, 32(1), pp. 668–680. doi: 10.1109/TPEL.2016.2527051.

Akagi, H., Kanazawa, Y. and Nabae, A. (1984). Instantaneous Reactive Power Compensatiors Comprising Switching Devices without Energy Storage Components. *IEEE Transactions on Industry,* IA-20(3), pp. 625–630. doi: 10.1109/TIA.1984.4504460.

Amin., Bambang, R. T., Rohman, A. S., Dronkers, C. J. and Ortega, R., Sasongko, A. (2014). Energy Management of Fuel Cell/Battery/Supercapacitor Hybrid Power Sources Using Model Predictive Control. *IEEE Transactions on Industrial Informatics,* 10(4), pp. 1192–2002. doi: 10.1109/TII.2014.2333873.

Ara´ujo, R. E., de Castro, R., Pinto, C., Melo, P. and Freitas, D. (2014). Combined Sizing and Energy Management in EVs with Batteries and Supercapacitors. *IEEE Transactions on Vehicular Technology*, 63(7), pp. 3062–3076. doi: 10.1109/TVT.2014.2318275.

Aredes, M. and Watanabe, E. H. (1995). New Control Algorithms for Series and Shunt Three-Phase Four-wire Active Power Filters. *IEEE Transactions on Power Delivery*, 10(3), pp. 1649–1656. doi: 10.1109/61.400952.

Dusmez, S. and Khaligh, A. (2014). A Supervisory Power-Splitting Approach for a New Ultracapacitor, Battery Vehicle Deploying Two Propulsion Machines. *EEE Transactions on Industrial Informatics*, 10(3), pp. 1960–1971. doi: 10.1109/TII.2014.2299237.

Henz, C. L. and Gasparin, F. P. (2021). Investigation on Control Strategies for a Single-Phase Photovoltaic Inverter Using PSCAD/EMTDC Software. *Power*

Electronics and Drives, 6(1), pp.75–99. doi: 10.2478/pead-2021-0006.

Hredzak, B., Agelidis, V. G. and Demetriades, G. D. (2014). A Low Complexity Control System for a Hybrid dc Power Source Based on Ultracapacitor–Lead–Acid Battery Configuration. *IEEE Transactions on Power Electronics*, 29(6), pp. 2882–2891. doi: 10.1109/TPEL.2013.2277518.

Huang, S. C., Tseng, K. H., Liang, J. W., Chang, C. L. and Pecht, M. G. (2017). An Online SOC and SOH Estimation Model for Lithium-Ion Batteries. *Energies*, 10(4), p. 512. doi: https://doi.org/10.3390/en10040512.

Jossen, A. (2006). Fundamentals of Battery Dynamics. *Journal of Power Sources*, 154(2), pp. 530–538. doi: 10.1016/j.jpowsour.2005.10.041.

Kollimalla, S. K., Ukil, A., Gooi, H. B., Manandhar, U. and Tummuru, N. R. (2017). Optimization of Charge/Discharge Rates of a Battery Using a Two-Stage Rate Limit Control. *IEEE Transactions on Sustainable Energy*, 8(2), pp. 516–529. doi: 10.1109/TSTE.2016.2608968.

Lahyani, A., Venet, P., Guermazi, A. and Troudi, A. (2013). Battery/Supercapacitors Combination in Uninterruptible Power Supply (UPS). *IEEE Transactions on Power Electronics*, 28(4), pp. 1509–1522. doi: 10.1109/TPEL.2012.2210736.

Łukasz, K. and Zieliński, D. (2021). Control of a Four-Wire Hybrid Prosumer Converter for Balancing Utility Grids. *Power Electronics and Drives*, 6(1), pp.1–11. doi: 10.2478/pead-2021-0001.

Ma, T., Yang, H. and Lu, L. (2015). Development of Hybrid Battery-Supercapacitor Energy Storage for Remote Area Renewable Energy Systems. *Applied Energy*, 153, pp. 56–62. doi: 10.1016/j.apenergy.2014.12.008.

Manandhar, U., Tummuru, N. R., Kollimalla, S. K., Ukil, A., Beng, G. H. and Chaudhari, K. (2018). Validation of Faster Joint Control Strategy for Battery- and Supercapacitor-Based Energy Storage System. *IEEE Transactions on Industrial Electronics,* 65(4), pp. 3286–3294. doi: 10.1109/TIE.2017.2750622.

Mukherjee, N. and Strickland, D. (2016). Control of Cascaded dc-dc Converter Based Hybrid Battery Energy Storage Systems – Part I: Stability Issue. *IEEE Transactions on Industrial Electronics*, 63(4), pp. 2340–2349. doi: 10.1109/TIE.2015.2509911.

Tremblay, O., Dessaint, L. A. and Dekkiche, A. I. (2007). A Generic Battery Model for the Dynamic Simulation of Hybrid Electric Vehicles. In: *Proceedings IEEE Vehicle Power and Propulsion Conference*, 284–289. doi: 10.1109/VPPC.2007.4544139.

Appendix

A1. Small-Signal Modelling of the Supercapacitor (SC)

Small-signal modelling of the SC-based DC–DC converter is shown, because the battery and SC-based DC–DC converter have similar circuit diagrams, with the result that the small-signal modelling will have the corresponding similar steps. Also in Fig. A1, the input voltage to the SC-based DC–DC converter is considered as v_{in} for general expression of input voltage to the DC–DC converter (i.e. $v_{in} = v_{sc}$ for SC DC–DC converter and $v_{in} = v_{bat}$ for battery DC–DC converter). For example, the equivalent circuit diagram of the battery DC–DC converter is shown in Fig. A2, where the input voltage is represented as v_{bat}.

$$X = \begin{bmatrix} i_{L_{sc}} & v_c \end{bmatrix}^T$$

$$Y = \begin{bmatrix} v_{dc} & i_{in} \end{bmatrix}^T$$

During $0 \le t \le d_{sc}T_{sw}$

$$\frac{di_{L_{sc}}}{dt} = \frac{1}{L_{sc}}.V_{in}$$

$$\frac{dv_c}{dt} = -\frac{1}{RC_{sc}}.v_c$$

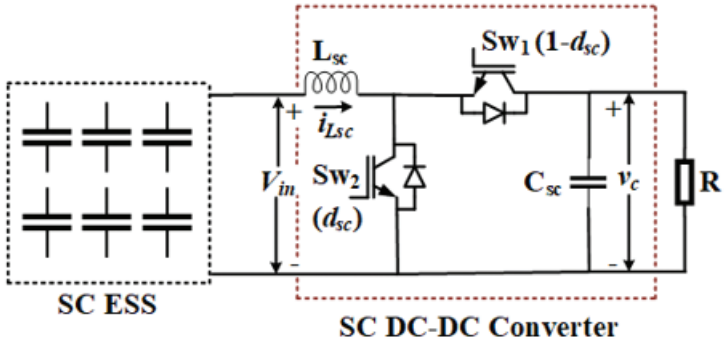

Fig. A1. Circuit diagram for small-signal modelling of the SC based DC–DC converter.

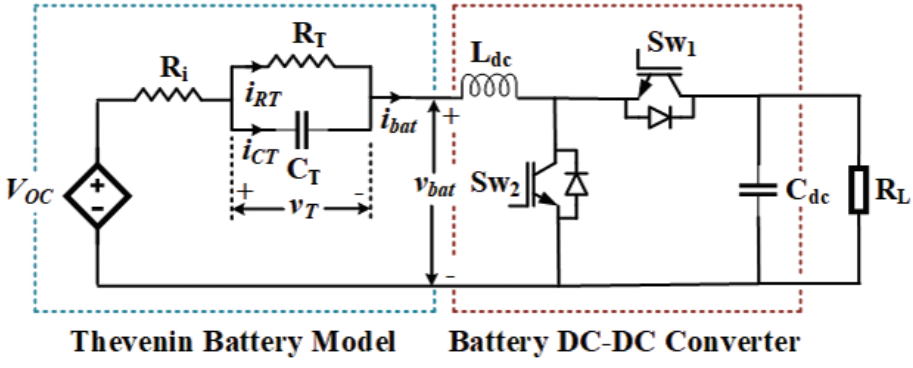

Fig. A2. Circuit diagram for small-signal modelling of the battery based DC–DC converter.

Therefore,

$$\begin{bmatrix} \frac{di_{L_{sc}}}{dt} \\ \frac{dv_c}{dt} \end{bmatrix} = \begin{bmatrix} 0 & 0 \\ 0 & -\frac{1}{RC_{sc}} \end{bmatrix} \begin{bmatrix} i_{L_{sc}} \\ v_c \end{bmatrix} + \begin{bmatrix} \frac{1}{L_{sc}} \\ 0 \end{bmatrix} V_{in}$$

During $d_{sc}T_{sw} \le t \le T_{sw}$

$$\frac{di_{L_{sc}}}{dt} = \left[-\frac{1}{L_{sc}} v_c + \frac{1}{L_{sc}} V_{in} \right]$$

$$\frac{dv_c}{dt} = \left[\frac{1}{C_{sc}} i_{L_{sc}} - \frac{1}{RC_{sc}} v_c \right]$$

Therefore, we obtain:

$$\begin{bmatrix} \frac{di_{L_{sc}}}{dt} \\ \frac{dv_c}{dt} \end{bmatrix} = \begin{bmatrix} 0 & -\frac{1}{L_{sc}} \\ \frac{1}{C_{sc}} & -\frac{1}{RC_{sc}} \end{bmatrix} \begin{bmatrix} i_{l_{sc}} \\ v_c \end{bmatrix} + \begin{bmatrix} \frac{1}{L_{sc}} \\ 0 \end{bmatrix} V_{in}$$

By state-space averaging, the following expression may be obtained:

$$A = A_1 d_{sc} + A_2 \left(1 - d_{sc}\right) = \begin{bmatrix} 0 & -\frac{\left(1-d_{sc}\right)}{L_{sc}} \\ \frac{\left(1-d_{sc}\right)}{C_{sc}} & -\frac{1}{RC_{sc}} \end{bmatrix}$$

$$B = B_1 d_{sc} + B_2 \left(1 - d_{sc}\right) = \begin{bmatrix} \frac{1}{L_{sc}} \\ 0 \end{bmatrix}$$

And,

$$\begin{bmatrix} v_{dc} \\ i_{in} \end{bmatrix} = \begin{bmatrix} 0 & 1 \\ 1 & 0 \end{bmatrix} \begin{bmatrix} i_{L_{sc}} \\ v_c \end{bmatrix}$$

Hence, state-space representation can be expressed as:

$$\begin{bmatrix} \frac{di_{L_{sc}}}{dt} \\ \frac{dv_c}{dt} \end{bmatrix} = \begin{bmatrix} 0 & -\frac{\left(1-d_{sc}\right)}{L_{sc}} \\ \frac{\left(1-d_{sc}\right)}{C_{sc}} & -\frac{1}{RC_{sc}} \end{bmatrix} \begin{bmatrix} i_{L_{sc}} \\ v_c \end{bmatrix} + \begin{bmatrix} \frac{1}{L_{sc}} \\ 0 \end{bmatrix} v_{in}$$

$$\begin{bmatrix} v_{dc} \\ i_{in} \end{bmatrix} = \begin{bmatrix} 0 & 1 \\ 1 & 0 \end{bmatrix} \begin{bmatrix} i_{L_{sc}} \\ v_c \end{bmatrix}$$

Using small-signal perturbation, we obtain:

$$i_{L_{sc}}(t)=\left[I_{L_{sc}}+\widehat{i_{L_{sc}}}(t)\right]$$

$$v_c(t)=\left[V_c+\widehat{v_c}(t)\right]$$

$$d_{sc}(t)=\left[D_{sc}+\widehat{d_{sc}}(t)\right]$$

$$v_{in}(t)+\left[V_{in}+\widehat{v_{in}}(t)\right]$$

Therefore,

$$\begin{bmatrix}\frac{d}{dt}\left(I_{L_{sc}}+\widehat{i_{L_{sc}}}\right)\\ \frac{d}{dt}\left(V_c+\widehat{v_c}\right)\end{bmatrix}=\begin{bmatrix}0 & \frac{\left(1-\left(D_{sc}+\widehat{d_{sc}}\right)\right)}{L_{sc}}\\ -\frac{\left(1-\left(D_{sc}+\widehat{d_{sc}}\right)\right)}{C_{sc}} & -\frac{1}{RC_{sc}}\end{bmatrix}\begin{bmatrix}I_{L_{sc}}+\widehat{i_{L_{sc}}}\\ V_c+\widehat{v_c}\end{bmatrix}+\begin{bmatrix}\frac{1}{L_{sc}}\\ 0\end{bmatrix}\left(V_{in}+\widehat{v_{in}}\right)$$

$$\text{or, }\begin{bmatrix}\frac{d}{dt}\widehat{i_{L_{sc}}}\\ \frac{d}{dt}\widehat{v_c}\end{bmatrix}=\left\{\begin{bmatrix}0 & -\frac{(1-D_{sc})}{L_{sc}}\\ \frac{(1-D_{sc})}{C_{sc}} & -\frac{1}{RC_{sc}}\end{bmatrix}\begin{bmatrix}I_{L_{sc}}\\ v_c\end{bmatrix}+\begin{bmatrix}\frac{1}{L_{sc}}\\ 0\end{bmatrix}V_{in}\right\}+\begin{bmatrix}0 & \frac{(1-D_{sc})}{L_{sc}}\\ \frac{(1-D_{sc})}{C_{sc}} & -\frac{1}{RC_{sc}}\end{bmatrix}\begin{bmatrix}\widehat{i_{L_{sc}}}\\ \widehat{v_c}\end{bmatrix}$$

$$+\begin{bmatrix}0 & \frac{\widehat{d_{sc}}}{L_{sc}}\\ -\frac{\widehat{d_{sc}}}{C_{sc}} & 0\end{bmatrix}\begin{bmatrix}I_{L_{sc}}\\ v_c\end{bmatrix}+\begin{bmatrix}\frac{1}{L_{sc}}\\ 0\end{bmatrix}\widehat{v_{in}}$$

$$\text{or, }\begin{bmatrix}\frac{d}{dt}\widehat{i_{L_{sc}}}\\ \frac{d}{dt}\widehat{v_c}\end{bmatrix}=\begin{bmatrix}0 & \frac{(1-D_{sc})}{L_{sc}}\\ \frac{(1-D_{sc})}{C_{sc}} & -\frac{1}{RC_{sc}}\end{bmatrix}\begin{bmatrix}\widehat{i_{L_{sc}}}\\ \widehat{v_c}\end{bmatrix}+\begin{bmatrix}\frac{V_c}{L_{sc}}\\ \frac{I_{L_{sc}}}{C_{sc}}\end{bmatrix}\widehat{d_{sc}}+\begin{bmatrix}\frac{1}{L_{sc}}\\ 0\end{bmatrix}\widehat{v_{in}}$$

$$\begin{bmatrix}\frac{d}{dt}\widehat{i_{L_{sc}}}\\ \frac{d}{dt}\widehat{v_c}\end{bmatrix}=\begin{bmatrix}0 & \frac{(1-D_{sc})}{L_{sc}}\\ \frac{(1-D_{sc})}{C_{sc}} & -\frac{1}{RC_{sc}}\end{bmatrix}\begin{bmatrix}\widehat{i_{L_{sc}}}\\ \widehat{v_c}\end{bmatrix}+\begin{bmatrix}\frac{1}{L_{sc}} & \frac{V_c}{L_{sc}}\\ 0 & -\frac{I_{L_{sc}}}{C_{sc}}\end{bmatrix}\begin{bmatrix}\widehat{v_{in}}\\ \widehat{d_{sc}}\end{bmatrix}$$

$$\begin{bmatrix}v_c\\ i_{in}\end{bmatrix}=\begin{bmatrix}0 & 1\\ 1 & 0\end{bmatrix}\begin{bmatrix}\widehat{i_{L_{sc}}}\\ \widehat{v_c}\end{bmatrix}$$

Therefore,

$$\frac{\widehat{i_{in}}(s)}{\widehat{d_{sc}}(s)}=\frac{\widehat{i_{L_{sc}}}(s)}{\widehat{d_{sc}}(s)}=C_2(sI-A)^{-1}.B_2$$

$$\text{or, } G_{id_{sc}}(s)=\begin{bmatrix}1 & 0\end{bmatrix}\begin{bmatrix} s & \frac{(1-D_{sc})}{L_{sc}} \\ -\frac{(1-D_{sc})}{C_{sc}} & \left(s+\frac{1}{RC_{sc}}\right)\end{bmatrix}^{-1}\begin{bmatrix}\frac{V_c}{L_{sc}} \\ -\frac{I_{L_{sc}}}{C_{sc}}\end{bmatrix}$$

$$\text{or, } G_{id_{sc}}(s)=\begin{bmatrix}1 & 0\end{bmatrix}.\frac{1}{\left\{s\left(s+\frac{1}{RC_{sc}}\right)+\frac{(1-D_{sc})^2}{L_{sc}C_{sc}}\right\}}.\begin{bmatrix}\left(s+\frac{1}{RC_{sc}}\right) & -\frac{(1-D_{sc})}{L_{sc}} \\ \frac{(1-D_{sc})}{C_{sc}} & s\end{bmatrix}\begin{bmatrix}\frac{V_c}{L_{sc}} \\ -\frac{I_{L_{sc}}}{C_{sc}}\end{bmatrix}$$

$$\text{or, } G_{id_{sc}}(s)=\frac{1}{\left\{s\left(s+\frac{1}{RC_{sc}}\right)+\frac{(1-D_{sc})^2}{L_{sc}C_{sc}}\right\}}.\begin{bmatrix}\left(s+\frac{1}{RC_s}\right)-\frac{(1-D_{sc})}{L_{sc}}\end{bmatrix}\begin{bmatrix}\frac{V_c}{L_{sc}} \\ -\frac{I_{L_{sc}}}{C_{sc}}\end{bmatrix}$$

$$\text{or, } G_{id_{sc}}(s)=\frac{\left\{\frac{V_c}{L_{sc}}s+\frac{V_{dc}/R}{L_{sc}C_{sc}}+\frac{I_{L_{sc}}}{C_{sc}}\frac{(1-D_{sc})}{L_{sc}}\right\}}{\left\{s\left(s+\frac{1}{RC_{sc}}\right)+\frac{(1-D_{sc})^2}{L_{sc}C_{sc}}\right\}}=\frac{\left\{(C_{sc}V_{dc})s+\frac{V_{dc}}{R}(2-D_{sc})\right\}}{\left\{(L_{sc}C_{sc})s^2+\left(\frac{L_{sc}}{R}\right)s+(1-D_{sc})^2\right\}}$$

And,

$$\frac{\hat{v}_{dc}(s)}{\hat{d}_{dc}(s)}=C_1(sI-A)^{-1}B_2=\begin{bmatrix}0 & 1\end{bmatrix}\begin{bmatrix} s & \frac{1-D_{sc}}{L_{sc}} \\ -\frac{(1-D_{sc})}{C_{sc}} & s+\frac{1}{RC_{sc}}\end{bmatrix}^{-1}\begin{bmatrix}\frac{V_c}{L_{sc}} \\ -\frac{I_{L_{sc}}}{C_{sc}}\end{bmatrix}$$

$$\text{or, } \frac{\hat{v}_{dc}(s)}{\hat{d}_{dc}(s)}=\begin{bmatrix}0 & 1\end{bmatrix}.\frac{1}{\left\{s\left(s+\frac{1}{RC_{sc}}\right)+\frac{(1-D_{sc})^2}{L_{sc}C_{sc}}\right\}}.\begin{bmatrix}s+\frac{1}{RC_{sc}} & -\frac{(1-D_{sc})}{L_{sc}} \\ \frac{(1-D_{sc})}{C_{sc}} & s\end{bmatrix}\begin{bmatrix}\frac{V_c}{L_{sc}} \\ -\frac{I_{L_{sc}}}{C_{sc}}\end{bmatrix}$$

$$\text{or, } \frac{\hat{v}_{dc}(s)}{\hat{d}_{dc}(s)}=\frac{1}{\left\{s^2+\frac{s}{RC_{sc}}+\frac{(1-D_{sc})^2}{L_{sc}C_{sc}}\right\}}.\begin{bmatrix}\frac{(1-D_{sc})}{C_{sc}} & s\end{bmatrix}\begin{bmatrix}\frac{V_c}{L_{sc}} \\ -\frac{I_{L_{sc}}}{C_{sc}}\end{bmatrix}$$

$$\text{or, } \frac{\hat{v}_{dc}(s)}{\hat{d}_{dc}(s)}=\frac{\left\{\frac{(1-D_{sc}).V_{dc}}{L_{sc}C_{sc}}-\frac{I_{L_{sc}}}{C_{sc}}.s\right\}}{\left\{s^2+\frac{s}{RC_{sc}}+\frac{(1-D_{sc})^2}{L_{sc}C_{sc}}\right\}}$$

$$\text{or, } G_{vd\_sc(s)} = \frac{\left\{\left(1-D_{sc}\right).V_{dc} - L_{sc}.\frac{V_{dc}}{R}.s\right\}}{\left\{\left(L_{sc}C_{sc}\right)s^2 + \left(\frac{L_{sc}}{R}\right)s + \left(1-D_{sc}\right)^2\right\}}$$

The outer voltage control loop may be obtained as the following expression:

$$G_{vi\_sc(s)} = \frac{\widehat{v_{dc}}(s)}{\widehat{i_{L_{sc}}}(s)} = \frac{\widehat{v_{dc}}(s)}{\widehat{d_{sc}}(s)} . \frac{\widehat{d_{sc}}(s)}{\widehat{I_{L_{sc}}}(s)}$$

$$\text{or, } G_{vi\_sc}(s) = \frac{\left\{\left(1-D_{sc}\right).V_{dc} - L_{sc}.\frac{V_{dc}}{R}.s\right\}}{\left\{\left(C_{sc}V_{dc}\right)s + \frac{V_{dc}}{R}\left(2-D_{sc}\right)\right\}}$$

$$\frac{\hat{v}_{dc}(s)}{\hat{v}_{dc}(s)} = \frac{\hat{v}_{dc}(s)}{\hat{v}_{sc}(s)} = C_1\left(sI-A\right)^{-1}B_1 = \begin{bmatrix}0 & 1\end{bmatrix}.\frac{1}{\left\{s\left(s+\frac{1}{RC_{sc}}\right)+\frac{\left(1-D_{sc}\right)^2}{L_{sc}C_{sc}}\right\}}.\begin{bmatrix}\left(s+\frac{1}{RC_{sc}}\right) & -\frac{\left(1-D_{sc}\right)}{L_{sc}} \\ \frac{\left(1-D_{sc}\right)}{C_{sc}} & s\end{bmatrix}.\begin{bmatrix}\frac{1}{L_{sc}} \\ 0\end{bmatrix}$$

$$= \frac{1}{\left\{s^2 + \frac{s}{RC_{sc}} + \frac{\left(1-D_{sc}\right)^2}{L_{sc}C_{sc}}\right\}}.\begin{bmatrix}0 & 1\end{bmatrix}\begin{bmatrix}\frac{1}{L_{sc}}.\left(s+\frac{1}{RC_{sc}}\right) \\ \frac{\left(1-D_{sc}\right)}{L_{sc}C_{sc}}\end{bmatrix} = \frac{\frac{\left(1-D_{sc}\right)}{L_{sc}C_{sc}}}{s^2 + \frac{s}{RC_{sc}} + \frac{\left(1-D_{sc}\right)^2}{L_{sc}C_{sc}}} = \frac{\left(1-D_{sc}\right)}{\left\{\left(L_{sc}C_{sc}\right)s^2 + \left(\frac{L_{sc}}{R}\right)s + \left(1-D_{sc}\right)^2\right\}}$$

Therefore,

$$G_{vv\_sc}(s) = \frac{\hat{v}_{sc}(s)}{\hat{v}_{dc}(s)} = \frac{\left\{\left(L_{sc}C_{sc}\right)s^2 + \left(\frac{L_{sc}}{R}\right)s + \left(1-D_{sc}\right)^2\right\}}{\left(1-D_{sc}\right)}$$

Similarly, for the consideration of small-signal modelling of battery, we obtain:

$$G_{vv\_bat}(s) = \frac{\hat{v}_{bat}(s)}{\hat{v}_{dc}(s)} = \frac{\left\{\left(L_{bat}C_{bat}\right)s^2 + \left(\frac{L_{bat}}{R}\right)s + \left(1-D_{bat}\right)^2\right\}}{\left(1-D_{bat}\right)}$$

Hence, for loop transfer function, the control loop can be formulated as follows:
Where,

$$G_{closed\ loop_{isc}}(s) = \frac{G_{PI_i}(s) * G_{id_{sc}}(s)}{\left[1 + G_{PI_i}(s).G_{id_{sc}}(s)\right]}$$

And, $G_{PI_i}(s) = \left[K_{Pi} + \frac{K_{Ii}}{s}\right] = \frac{sK_{Pi} + K_{Ii}}{s}$